PIXE ANALYSIS OF OIL-PAINT PIGMENTS:

PROOF OF PRINCIPLE

by

Benjamin T. Hall

A senior thesis submitted to the faculty of

Brigham Young University

in partial fulfillment of the requirements for the degree of

Bachelor of Science

Department of Physics and Astronomy

Brigham Young University

April 2006

BRIGHAM YOUNG UNIVERSITY

DEPARTMENT APPROVAL

of a senior thesis submitted by

Benjamin T. Hall

This thesis has been reviewed by the research advisor, research coordinator, and department chair and has been found to be satisfactory.

Date	Lawrence B. Rees, Advisor
Date	Jean-Francois Van Huele, Research Coordinator
Date	Scott D. Sommerfeldt, Chair

ABSTRACT

PIXE ANALYSIS OF OIL-PAINT PIGMENTS:

PROOF OF PRINCIPLE

Benjamin T. Hall

Department of Physics and Astronomy

Bachelor of Science

In this thesis we present a proof of principle for the construction of pigment databases to facilitate the analysis of paintings using Particle-Induced X-ray Emission (PIXE) spectroscopic techniques. A small data set is constructed using internal-beam PIXE on 10 modern pigments. We compare this data set to the data obtained from thick targets made from combinations of these same pigments analyzed using external-beam mode in a helium atmosphere. We show that the data set accurately predicts the composition of six of the eight targets. Limitations such as charging-induced background, the inability to resolve layering, and thickness-caused inaccuracies are discussed.

ACKNOWLEDGMENTS

We would like to thank Dr. Lawrence Rees for advising us on this project. We would also like to acknowledge the use of Dr. Delbert Eatough's clean room for the preparation of targets. Our thanks go to the Office of Research and Creative Activities at Brigham Young University for providing supplementary funding. We thank the Department of Physics and Astronomy for being the primary provider of equipment and funding for this project.

Contents

List of Figures

Chapter 1

Introduction

1.1 Methods and purposes of pigment analysis

Artistic analysis has been around as long as art itself. Art scholars have dissected paintings, debating nuances of style, medium and effect of paintings. The scholars have commonly used both stylistic and quantitative methods. The rapid advance of scientific analysis techniques in the 20^{th} century has led to a rise in the number and importance of quantitative studies of artwork.

Also since ancient times, cunning artists have tried to cash in on the popularity of the master painters by creating works of art that appear to be genuine masterpieces, but are merely forgeries. An example of this is a painting by Dutch forger Hans van Meegeren titled "Christ and the Disciples at Emmaus"(Fig. 1.1). This forgery was perpetrated in the mid-1930s in the style of famous Dutch painter Jan Vermeer. An example of an authentic Vermeer, "Officer and Laughing Girl" is shown in Fig. 1.2. Most of the Dutch art establishment accepted the forgery as genuine for many years; Van Meegeren eventually admitted to the forgery of this and several other paintings and was sentenced to two years in prison [1].

Figure 1.1 Hans van Meegeren's "Christ and the Disciples at Emmaus" [1]

Figure 1.2 Vermeer's "Officer and Laughing Girl"

The forgoing discussion illustrates the need for better methods to date and to authenticate the provenance of paintings. Stylistic analysis commonly involves analyzing the methods of painting and the characteristic brush patterns [2]. This is a highly developed field and is beyond the scope of the current thesis. Such analysis is complicated by its non-quantitative nature and lack of absolute precision.

With the development of modern chemistry and physics, it is now possible to analyze the pigments used in the painting. Knowing the composition can verify the authenticity of the painting—for example, titanium-based white pigments only have been used since the 1930's. Before this, white colors were produced with lead-based pigments. Thus, if more than trace amounts of titanium are found in a supposedly Renaissance-era painting, the painting is either a fraud or has been recently restored using modern paints. In this way, pigment analysis forms a negative check on authenticity. We do not want to see traces of modern pigments in ancient paintings. Pigment analysis methods include the study of the crystalline structure of the pigments using optical microscopy, chemical assaying, electron microscopy, and Particle-Induced

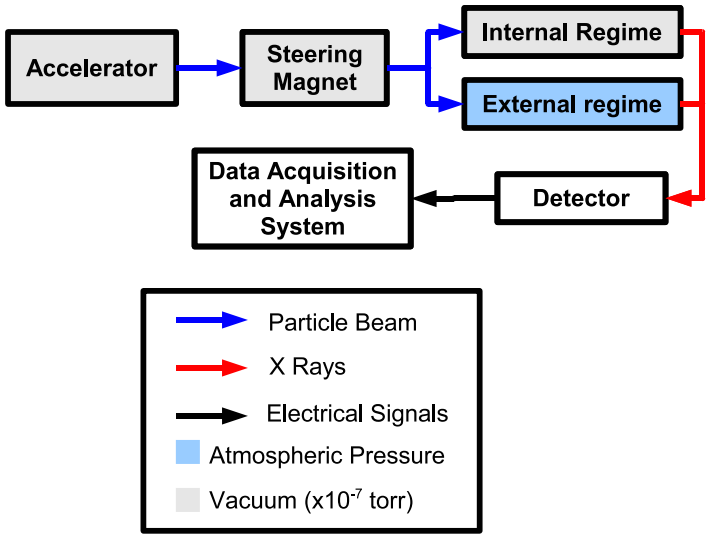

Figure 1.3 Schematic of particle-induced x-ray emission process

X-ray Emission (PIXE) among others. Books have been written on the various analytical techniques [3, 4]; this thesis will focus only on PIXE.

1.2 What is PIXE?

The analytical process of particle-induced x-ray emission is outlined in schematic form in Fig. 1.3. Particles are accelerated and collide with the specimen, temporarily ionizing it. Electrons fill the holes thus created in the electronic orbitals, releasing X rays with energies characteristic of the element. X-ray detectors in concert with data acquisition systems produce an emission spectrum of counts versus energy. Software packages take this spectrum and convert it to elemental concentrations. A typical spectrum is shown in Fig. 1.4. The plot shows total x-ray counts versus energy—the area under each peak is proportional to its elemental concentration. The spectral lines corresponding to each of the major elements are labeled—the double peaks for

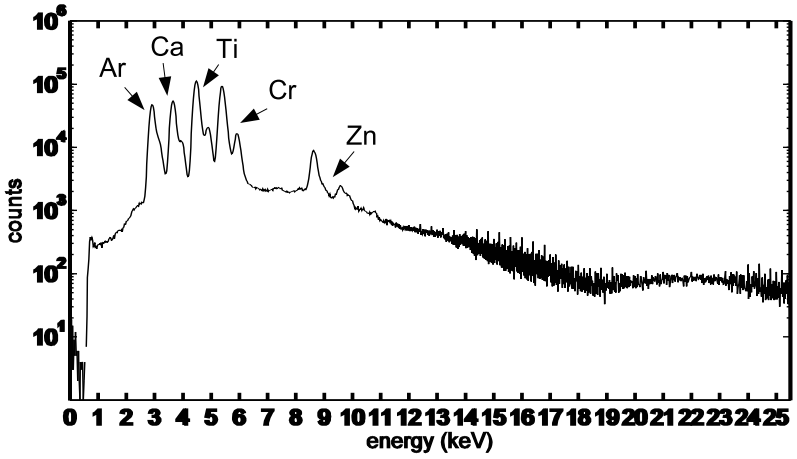

Figure 1.4 Semi-log spectrum of Chromium Oxide Green mixed with Titanium White

each element are characteristic of two types of x-ray transitions (see section 2.5 for more details on interpreting the spectra).

All of the above applies equally well to all PIXE systems. The systems differ in which particle is to be accelerated, at what energy, and whether the target is contained in the beam line and thus in vacuum or not. Particles to be accelerated range from single protons to ions as heavy as U^{235}. Energies range from 1 to about 68 MeV—above this energy the interaction cross-section becomes too small to effectively generate X rays. Different focusing regimes exist–the tightest focus is around $50\mu m^2$, compared to a beam area of about 30 mm^2 for PIXE without extra focusing. Tight focus allows the operator to chose his target area very precisely without including extraneous points in the sample.

1.3 Why PIXE?

PIXE has several advantages over other trace-element analysis techniques. First, it is almost completely nondestructive. When used on thick media (such as paintings) no significant damage is done [5]. This means that no permanent changes visible to the eye are made. Most commonly paintings are examined in standard atmospheres; the particle beam exits the evacuated beam line before encountering the target. Paintings to be analyzed in this manner do not have to be vacuum-stable. This compares favorably to standard chemical techniques, which require the destruction of a small piece of the object under study. Second, when properly used, PIXE can distinguish and quantify elemental concentrations as low as 0.1 part per million, depending on the element. This high sensitivity allows differentiation of subtly different pigments. Third, properly equipped PIXE laboratories can "scan" the surface of a painting, creating a spatial profile of selected regions of the object [6]. Fourth, PIXE techniques lend themselves well to the creation of large data sets of pigments; automated systems can thus be created to compare the compositions obtained from a questionable artwork to the database in order to determine the exact pigments used in the piece's composition and thus date or authenticate the painting.

PIXE also has several drawbacks. First, it requires a particle accelerator, thus making it impractical for most museums, as accelerators are expensive and difficult to maintain. Second, PIXE cannot easily detect elements lighter than aluminum (X rays from lighter elements are absorbed by the target and are thus not detected), making it of no use on purely organic pigments, although it can detect organometallic compounds. Third, PIXE cannot differentiate between compounds of elements with the same molecular formula as the perturbation of energy levels due to bonding is too small (about 10 eV) to make a difference in the energies of emitted X rays (these

X rays are in the keV scale). Last, the particles quickly lose energy in solid media, limiting the penetration depth to about 50 μm for 2 MeV protons. This difficulty can be partially overcome by increasing the energy of the beam, but this can reduce the ionization cross-section of the beam, thus reducing the number of X rays produced. In spite of the disadvantages, PIXE has much promise as a technique for analyzing art pigments.

Much current research into pigments and paintings using PIXE focuses on differential techniques, whereby the energy of the incident beam is varied, thus varying the penetration depth; information on different layers can thereby be acquired. N. Grassi at the University of Florence analyzed the Da Vinci's "Madonna dei Fusi" (Fig. 1.5) in 2004 using such a technique to create a depth profile of the painting—the analysis gives added insight to the layering methods used by the master artist [7].

Figure 1.5 Leonardo Da Vinci's "Madonna dei Fusi"

M. Sanchez del Rio *et al* [8] studied Mayan mural fragments using the AGLAE accelerator located at the Louvre museum in France, specifically looking at the use of the Maya Blue pigment, a type of indigo. In their work, they showed that PIXE

could be used to identify unknown pigments from their elemental composition.

1.4 PIXE at BYU

The Department of Physics and Astronomy at Brigham Young University (BYU) has a research group dedicated to trace-element analysis using PIXE and other related techniques. This group, to which I belong, is headed by Professor Lawrence Rees and is currently engaged in several analysis projects.

One of our longest-standing projects is a collaboration with Professor of Biology Larry St. Clair involving an attempt to use lichens to determine and track air pollutants. He and his students gather lichens from areas around the Intermountain West area of the United States and we process them in conjunction with the Department of Statistics to determine which lichen species are most suited for the role of living pollution monitors. We do most of the analysis and Dr. St. Clair is responsible for the biological interpretation of the data.

Other group members are engaged in various studies. One is currently studying how PIXE can be used as a forensic tool to analyze lead from bullets found at crime scenes. Another is studying the composition of inks found in 18^{th} and 19^{th} century books. A third is planning a project to correlate trace elements found in hair samples to male pattern baldness.

PIXE at BYU is carried out using a 2.17 MeV Van de Graaff proton accelerator with both external and internal modes available. The equipment is housed in BYU's underground laboratory facility. A view of the accelerator with the housing removed is shown in Fig. 1.6. Data are collected and analyzed with GUPIX, a software package that converts peak area to elemental compositions and produces background-subtracted compositions accurate to a few parts per million.

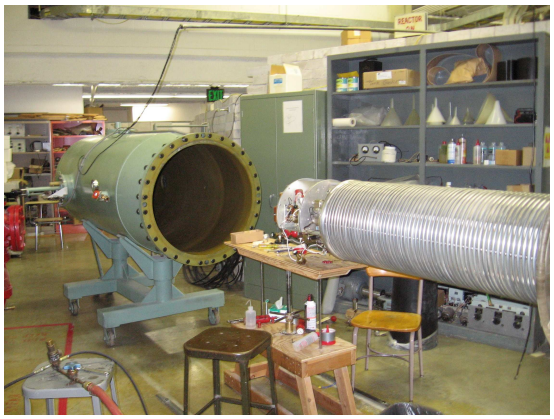

Figure 1.6 Photo of the BYU accelerator with tank open

1.5 Pigment analysis with PIXE at BYU

In this thesis we set out the details necessary to create a data set of pigments ancient and modern against which to compare paintings. We do not intend to actually create a comprehensive baseline—instead we propose a method, build a small data set, and show that this baseline is useful for deciphering data from more realistic samples.

Our data set consists of ten modern pigments in five colors. We process these pigments with internal beam PIXE, being careful to avoid cross-contamination. After creating this baseline, we prove its applicability to less carefully controlled specimens—paintings are not created in clean rooms and pigments are often mixed together to form new colors. We brush pigments onto standard art board and analyze these samples in the external regime in a helium atmosphere. External-beam analysis is the standard regime for object analysis.

1.6 Organization of thesis

In Chapter 2 we discuss the preparation and analysis of samples. Section 2.1 covers the choice of pigments for the trial database. Section 2.2 outlines the methods used in creating the targets for the database. Section 2.3 discusses how we make a more realistic set of targets to check against the database. In section 2.4 we discuss the equipment used and the procedure for obtaining spectra from the targets. Finally, section 2.5 details the procedure for turning the spectra into compositional data.

Chapter 3 contains the results and conclusions obtained from this project. We display and discuss the spectra for the targets in section 3.1.6. All the baseline targets' spectra are displayed; only selected spectra from external targets appear. We compare the internal results to the external ones in section 3.2 and draw conclusions in section 3.3. Limitations of this research and suggestions for further study are presented in section 3.4.

The appendix contains ancillary data such as tables of H-value corrections (section A.1) and presents the elemental concentration tables for the internal targets (section A.2).

Chapter 2

Establishing a Better Baseline

2.1 Choosing the baseline set

We make no attempt to create a data set containing all major pigment types—such a baseline is beyond the scope of this thesis as there exist hundreds of common pigments. To provide the greatest cross-section of pigments, we include several types of pigments—some are almost pure compounds of a single element (i.e. Prussian Blue), while others are made from compounds of many elements (i.e. Manganese Blue). This range provides a broader baseline against which to compare selected paintings. All the pigments selected are modern pigments, not the preparations used by artists in earlier centuries. This omission does not reduce the generality of the results obtained by the present research, as the target preparation techniques and analysis procedures remain the same with other pigments.

We chose two pigments in each of five colors for the present proof of principle. The choice of pigments and colors is essentially arbitrary, but we contend that these pigments form a reasonably representative set of commonly-used modern pigments. The common names of the pigments chosen are arranged by color in Fig. 2.1. The

Color	Pigments included in present study
Red	Cadmium Red, Primary Red
Blue	Prussian Blue, Manganese Blue
Green	Chromium Oxide Green, Veridian
White	Titanium White, Zinc White
Black	Ivory Black, Mars Black

Figure 2.1 Table of pigments included in baseline.

common names are somewhat misleading—they do not always correlate to the makeup of the pigment. As an example, Manganese Blue has no detectable concentrations of manganese. All the pigments chosen are basic pigments (as opposed to pigments made from mixtures of other pigments) which can be mixed to create various shades (see section 2.3 for examples).

2.2 Making the targets

The targets used in this thesis are divided into two types: thick and thin. A thick target is one where the protons cannot penetrate the entire sample and reach the Faraday cup (located behind the target) to be counted. These are commonly run externally (i.e. in atmosphere). "Thick" in this instance greater than the penetration distance of 2 MeV protons in solids, about 50 μm. Thin targets ($<$ 50 μm) are analyzed inside the primary beam line in vacuum, reducing the number of background X rays and also allowing higher proton energies on target. Protons can penetrate thin targets, allowing an direct count of the number of protons hitting the target. With our system, beam flux cannot be determined except at the end of the beam line,

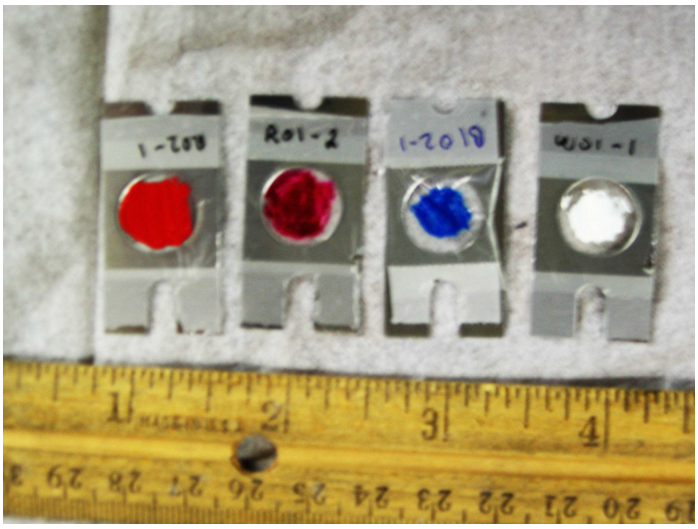

Figure 2.2 Photo of paint samples used to establish baseline set

in the Faraday cup. Thus, for thick targets, total charge on target is not directly measurable because most of the protons are stopped by the target and never reach the Faraday cup; we run these targets for a fixed time, usually 10 minutes, instead of running for a fixed total charge, as with thin targets.

The baseline set is composed of thin samples (Fig. 2.2). We created these targets by stretching 6 μm thick polystyrene film over aluminum frames to provide a stable base for the targets. These empty frames are weighed. Paint is then applied to the film with a glass rod and the frame is weighed again. The mass of paint, divided by the area covered by the paint, gives the thickness of the target in micrograms per square centimeter. This factor is the "thickness correction" used in data analysis (see section 2.5 for more details). To preserve thinness, we apply only 3-10 μg of paint per frame. We make two targets for each color to check reproducibility. The paint is then allowed to dry for several days at room temperature.

All of the above is done in a clean room to avoid contamination. All tools (paint holders, rods, etc.) are cleaned by immersion for several hours in "Micro-clean"

cleanser—this detergent is specially designed for cleaning trace-element equipment as it has constituents that bond with and remove metals, while the rest of the detergent removes nonmetallic elements. After immersion, the tools are rinsed in water filtered by a MilliQ system to remove most impurities.

2.3 Creating more realistic targets

We expended much effort to prevent contamination of the targets used for the baseline. Artists, however, rarely work in a clean room, and even more rarely clean their brushes and canvases in Micro-clean or wash with hyper-pure water. Pigments are also mixed together to form new colors. These considerations raise the question of applicability of the baseline data to real paintings. If the paintings are heavily contaminated, the contaminants may drown out the elemental fingerprints of the real pigments. We want the baseline to contain only the real pigments, so relaxing the contamination protocols is contraindicated. Mixing the pigments may overlap the spectral peaks, obscuring the true nature of the pigment.

To address the considerations of applicability, contamination, and mixing we prepared a set of samples under more realistic conditions. We cut standard painter's board into approximately 8 in by 2 in sections and divided each section into 2 in by 2 in squares. This is done for ease of analysis (no need to allow for large ranges of motion when changing targets). Paint is placed on a plastic palette and then applied to the board with a synthetic-fiber brush in the same manner as used by artists. Fig. 2.3 shows the completed targets. We clean the brush between colors in art grade mineral spirits and tap water. This procedure is designed to obviate the concerns about applicability and contamination. We show in section 3.1.6 that the baseline allows accurate prediction of the composition of these realistic samples.

Figure 2.3 Photo of single-color targets for external-beam analysis

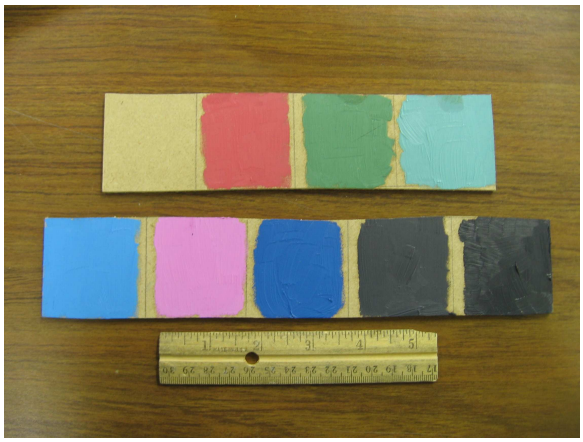

Figure 2.4 Photo of mixed-color targets for external-beam analysis

One of the most common reasons for mixing pigments is to lighten or darken the color. This is performed by mixing the colored pigment with white or black. To reproduce this effect, we prepared eight additional targets according to the realistic conditions described above. The paint used for these targets was a mixture of an individual color with the Titanium White pigment analyzed in the baseline. Titanium White is a commonly-used modern white pigment, and so makes an appropriate base for the other colors. We did not mix the two white pigments. Fig. 2.4 shows these mixed-color targets. By analyzing these targets, we show that the baseline technique

can accurately identify the constituent pigments of mixed paints in most cases and can quantify the proportions of pigments used.

2.4 Preparing for analysis

The equipment used for internal-beam analysis is shown in Fig. 2.5. Protons are steered into the internal branch of the beam line by the steering magnet (which also reduces the inevitable spread in proton energies by only bending those with the right energy to the beam line) and are collimated and aligned again. The target arm holds seven samples at a time, so that multiple runs can be completed without bringing the beam line to atmosphere pressure to change samples. Each target is run twice—each run with a different filter. The filter is not placed in the beam; the filter covers the detector window, shielding it from excess x-ray flux. Fig. 2.6 shows how the targets and filters are placed relative to the beam line and detector. The first run places a "pinhole" filter between target and detector. The pinhole filter is composed of a layer of beryllium over mylar with a pinhole in the mylar. This run requires low beam currents to avoid overloading the detector with X rays, but shows the lighter elements cleanly. On the second run we place a 0.71 μm thick mylar filter between target and detector; this filter reduces the number of counts per second seen (thus reducing the load on the detector), but allows higher beam currents and focuses on the heavier elements (i.e. those above calcium). The two runs are compared; for our targets there was no substantive difference between the results obtained (section 3.1.1). Our laboratory uses a lithium-drifted silicon crystal cooled with liquid nitrogen to convert the X rays into a current signal proportional to the energy of the detected photon. A computer running Canberra Inc.'s GENIE 2000 software reads the voltages and produces a list of total counts versus energy which is displayed on-screen. This display

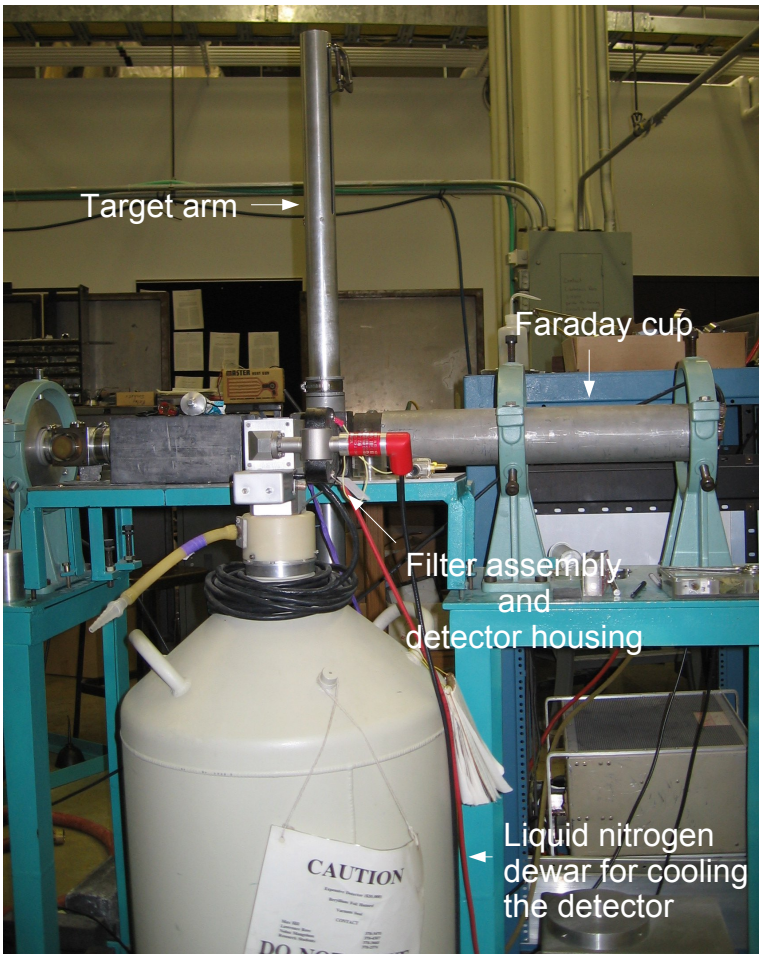

Figure 2.5 Photo of internal-beam setup showing locations of major pieces of equipment

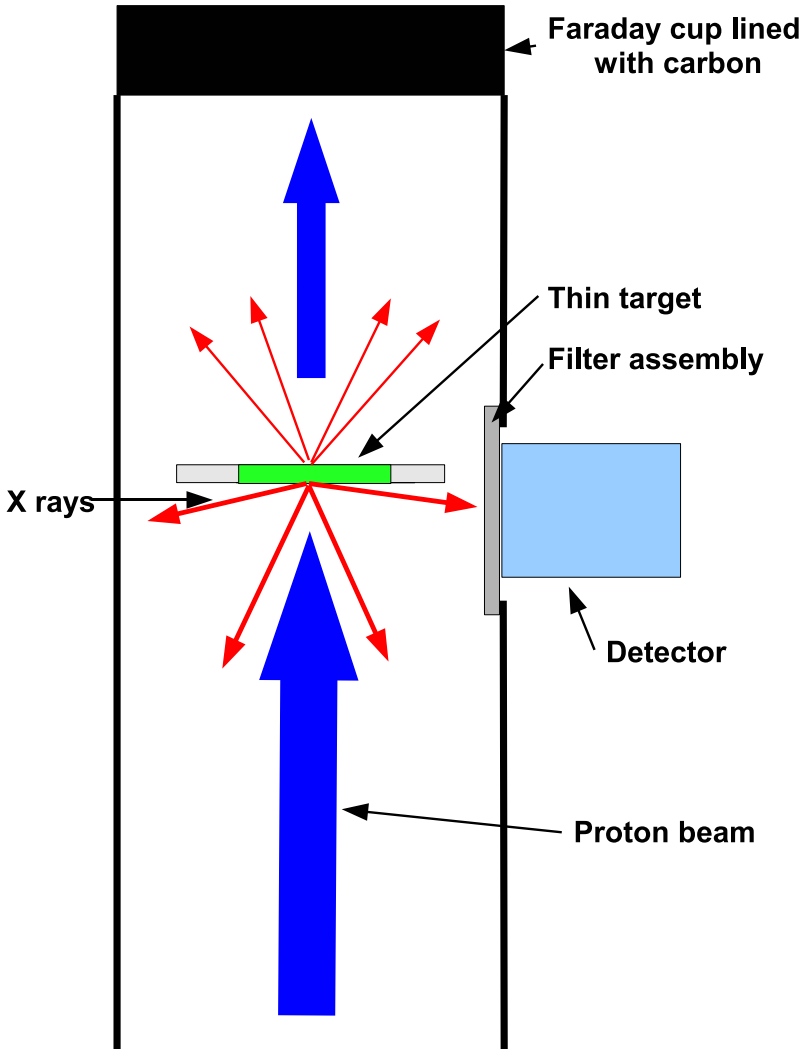

Figure 2.6 Drawing of inside of beam line placement the target, filter, and detector

is updated in realtime, so a qualitative description of the composition can be obtained without extensive analysis. For more precise data, however, some manipulation and fitting is required. Section 2.5 details how these data are converted into elemental concentrations.

In external mode, the beam is steered to the other branch of the beam line, which ends in a proton-permeable (but airtight) Kapton foil cap or window. This allows the protons to exit to atmosphere (or in our case a helium-filled bag), losing some energy (about 200 keV) in the window. The target and detector are positioned close to the end of the beam line, with the normal from the target surface bisecting the angle formed by the detector and beam line. The external system uses a hyper-pure germanium detector instead of the lithium-drifted silicon one used internally—the sensitivities are not substantially different and any variation is accounted for in the analysis process. This setup is shown in Fig. 2.7. All the data acquisition equipment is the same as for the internal setup. These targets are run for a fixed time (usually 15 minutes) at a known beam current in order to determine the charge deposited.

2.5 Turning raw data into organized elemental compositions

X rays that contribute to the spectrum fall into several classes based on the type of transition that produces them and must be handled separately in analysis. Kα and Kβ x rays come from the K (innermost) electron shell and dominate the spectrum. Heavier elements have prominent L lines, coming from transitions within the L shell.

Because the relations between the incoming protons and the emitted X rays are complex, a computer modeling system is required for analysis. We use GUPIX, one of the more standard systems. GUPIX takes information about the detector such as the

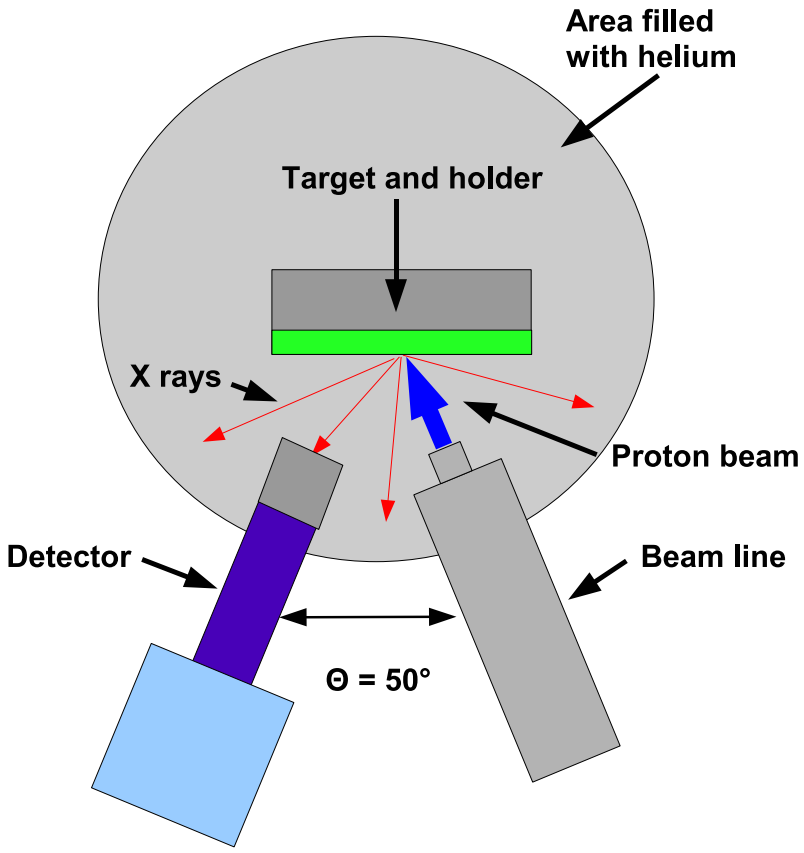

Figure 2.7 Diagram of external setup showing detector, target assembly, and the angle between detector, and beam line

solid angle between detector and beam and type of detector, information about the current run (energy of incident protons, thickness corrections, and charge on target) and the data from the data acquisition system about peak area, number of counts, etc. and transforms it into a scaled set of elemental compositions with least-squares error estimations. All of these transformations can be modeled by the following equation:

$$C = \frac{A}{H \times Q \times e \times Y \times f \times I} \tag{2.1}$$

where C is the concentration of the given element, A is the area under the background-subtracted peak corresponding to that element, H is an experimentally determined calibration constant (a constant for each detector setup), Q is the amount of charge on target, e is the detector efficiency at the energy of the peak, Y is the theoretical yield measured in counts per microcoulomb, f is the filter transmission at that energy, and I is the ionization cross-section for protons striking the given element. In practice, H takes into account e and f as well as the detector specific calibration information [9]. H is determined using standards with known concentrations of several elements and is constant for each accelerator and detector setup but depends on the element.

After GUPIX processing, we compensate for the non-uniformity of H by dividing the compositions of the elements by a correction factor. This correction factor is obtained by analyzing reference standards provided by the National Institute of Standards and Technology (NIST); the compositional data provided by NIST is compared to the data obtained locally to determine the correction needed for our equipment. See the appendix (A.1) for plots of H as a function of x-ray energy. We import the data into MATLAB (a numerical mathematics package) to plot and overlay spectra and to compare composition data between samples.

Chapter 3

Results and Conclusion

3.1 Spectra of targets

The pigments are treated individually in separate subsections arranged by color. In all successive spectra, spectral lines (Kα, Kβ, Lα) are not separately labeled; separately identifying the lines is only necessary for heavy elements such as lead—the others only have K lines and they are closely spaced in energy, eliminating confusion.

3.1.1 Red pigments

Primary Red is a magenta-colored pigment that we obtained from Maimeri Inc. It is shown in Fig. 2.3 on the far right in the second row. It is primarily composed of silicon, calcium, iron, and zinc, in decreasing order of concentration. The spectra obtained using the two filters are shown overlaid in Fig. 3.1. The two spectra match closely, showing that all the constituent elements are confined to those below zinc—otherwise the mylar-filtered run would show extra peaks at high energies. The differences in peak height come from the fact that the integrated charge differed between runs and that mylar filters a greater amount at low energy than does the pinhole filter.

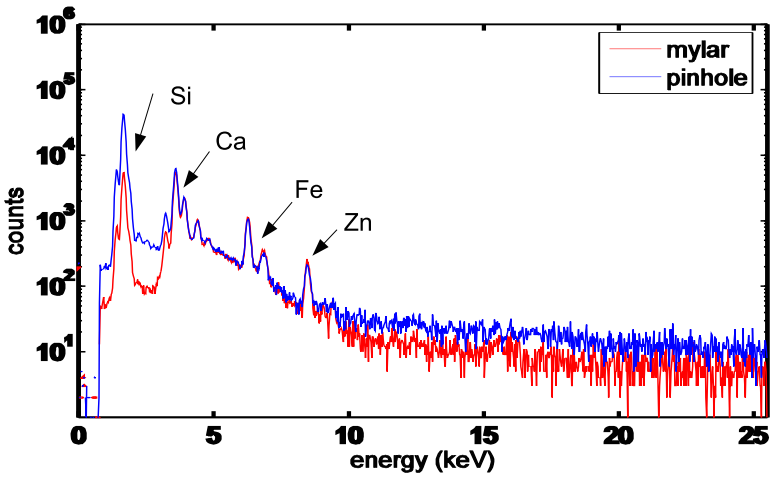

Figure 3.1 Spectrum of Primary Red showing major elements

Table A.1 contains the elemental compositions of this pigment.

The other red pigment, called Cadmium Red, is a orange-red pigment we obtained from M. Grahm and Co. It is shown in Fig. 2.3, second from the right in the first row. The concentration numbers (Table A.2) are quite suspect—the fit was quite poor (i.e. a χ^2 of 205, compared to the usual χ^2 of about 10). We do not know why this was so bad, but suspect that the target was so thick that the detector was swamped by X rays. Future experiments may want to examine this pigment more specifically, with an eye to reducing target thickness. The spectrum of this pigment is quite busy, with many peaks present at many energies.

3.1.2 Blue pigments

Manganese Blue is misnomer—there is no manganese present. As is evident from comparing the spectrum (Fig. 3.3) with the spectrum for Zinc White (Fig. 3.8), this pigment is composed of a mixture of pigments—a copper-based blue (giving the aluminum, copper, and iron peaks) and a zinc-based white (providing the calcium, titanium, and zinc peaks). Manganese Blue is royal blue in color and was obtained

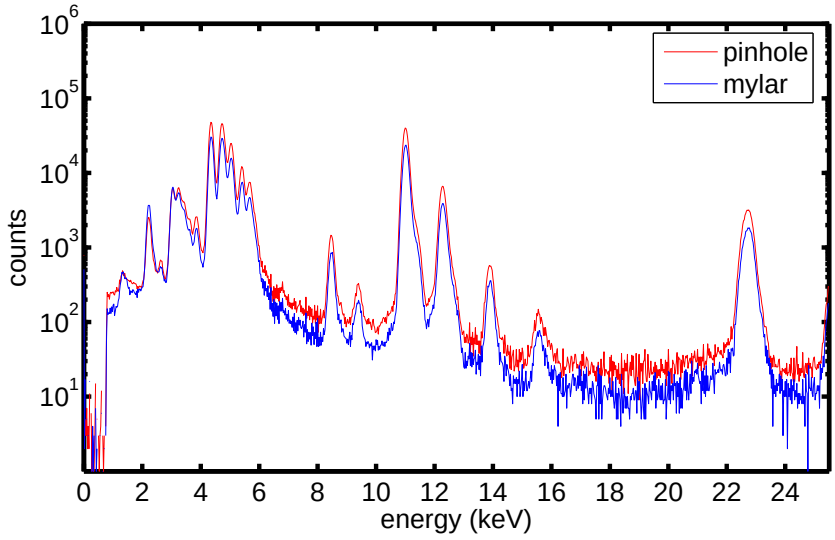

Figure 3.2 Spectrum of Cadmium Red showing major elements

from M. Grahm and Co. It is shown in Fig. 2.3 on the far right in the second row. Table A.3 contains the elemental compositions of this pigment.

Prussian Blue is a pigment dominated by iron. In color, it is a very dark blue, darker than navy blue, almost black when applied thickly. It is shown in Fig. 2.3, second from the right in the second row. It was obtained from M. Grahm and Co. The spectrum shows a spurious set of peaks at about 13 keV, exactly double the energy

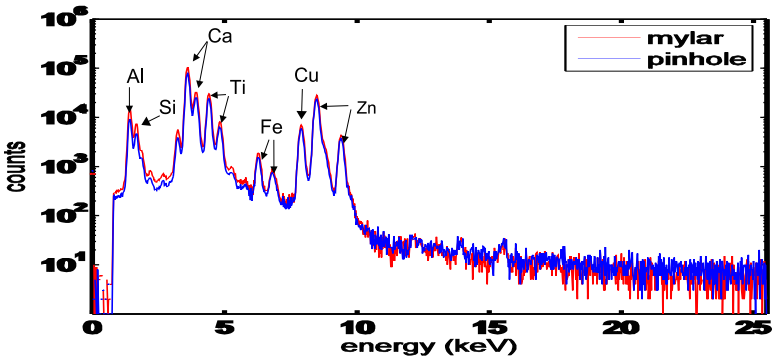

Figure 3.3 Spectrum of Manganese Blue showing major elements

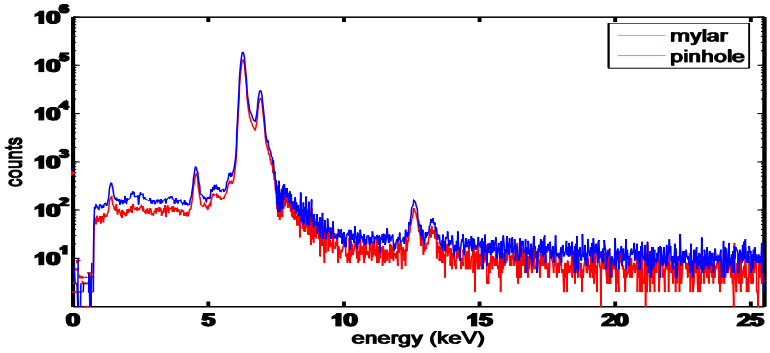

Figure 3.4 Spectrum of Prussian Blue showing major elements

of the major iron peaks. This phenomenon is called "sum-peaking," and is caused when too many X rays of a single energy enter the detector simultaneously, causing the detector to register two low-energy X rays as a single X ray of twice the energy. Fortunately, GUPIX compensates for these peaks when analyzing the spectra. The only danger in them is if they overlap and obscure real peaks. Table A.4 contains the elemental compositions of this pigment.

3.1.3 Green pigments

One element characterizes the two green pigments in the sample set—chromium. One pigment, Chromium Oxide Green, in fact, shows little else but chromium. Table A.5 shows the lack of any element except chromium in any but trace amounts. Chromium Oxide Green was obtained from Utrecht Inc. The spectrum (Fig. 3.5) exhibits both the sum-peaking effect discussed earlier as well as a peak called a "silicon escape peak." This artifact is only found when using a silicon-based detector, and is caused when a large number of X rays enter and ionize the silicon in the detector, causing it to read X rays at 1.7 keV lower than the incident energy. Like the sum-peaking, GUPIX corrects for this, but these peaks can obscure real elements.

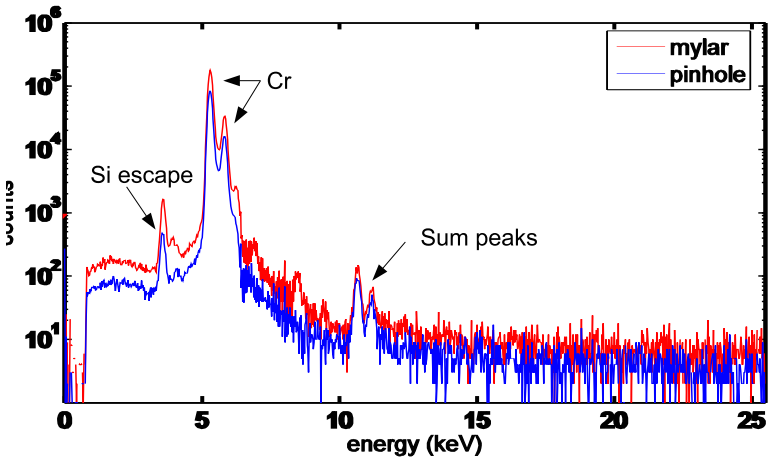

Figure 3.5 Spectrum of Chromium Oxide Green showing major elements

The other green pigment selected is known as Viridian. It too is dominated by chromium. Viridian is a turquoise green obtained from Utrecht Inc, and is shown in Fig. 2.3, second from the left in the second row. Table A.6 gives its elemental composition.

3.1.4 White pigments

White pigments are major constituents of many paints—as we have seen, zinc-based whites are used in the formation of other pigments such as Manganese Blue. There are two commonly used whites: titanium-based and zinc-based. Actually, as the spectra show, titanium whites are created by adding titanium to regular zinc pigments (Figs. 3.7 and 3.8). Also present are calcium and silicon. Titanium White is a more opaque pigment, with about equal proportions of titanium and zinc. See Table A.7 for a more exact composition. This pigment, as well as Zinc White, was obtained from M. Grahm and Co. The pigments are shown on the first row of Fig. 2.3.

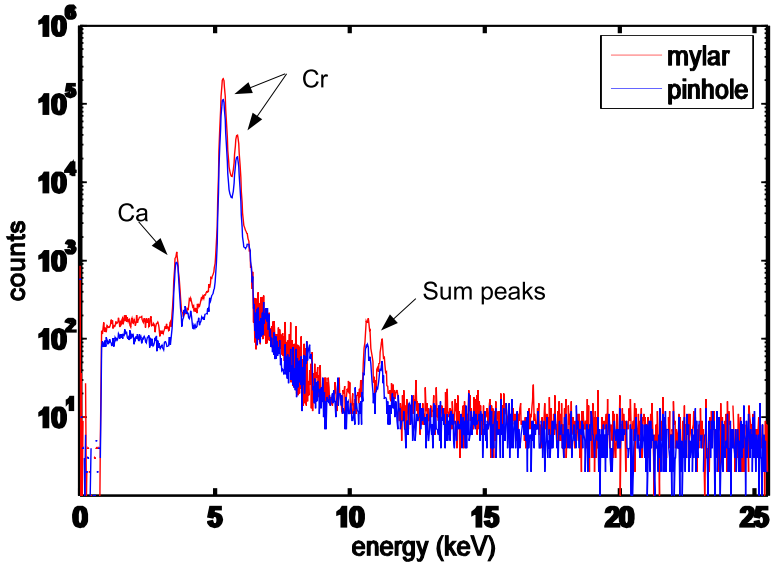

Figure 3.6 Spectrum of Viridian showing major elements

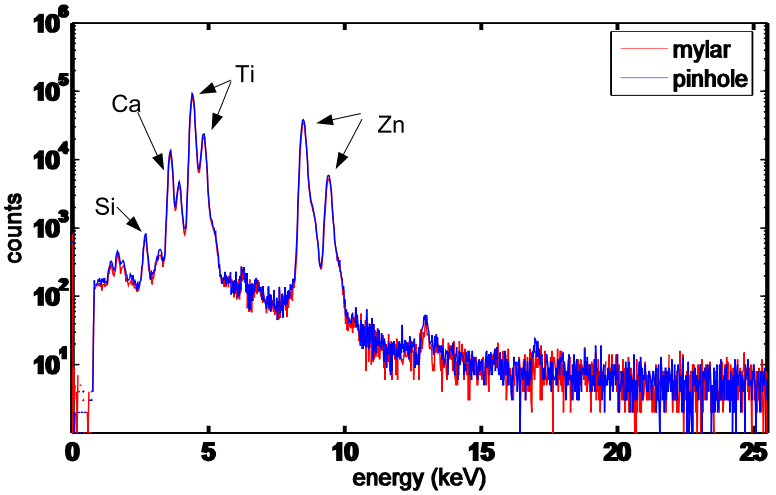

Figure 3.7 Spectrum of Titanium White showing major elements

3.1.5 Black pigments

Both black pigments, while very different in composition, are similar in color. They are shown in the top row of Fig. 2.3. Both were obtained from Utrecht Inc. Ivory Black is primarily composed of calcium with some iron and potassium (table A.9), while Mars Black is dominated by iron, with small amounts of manganese and calcium (Table A.10). As we show in section 3.2, Ivory Black is not well distinguishable from Titanium White when mixed—the combined spectrum shows only the white pigment.

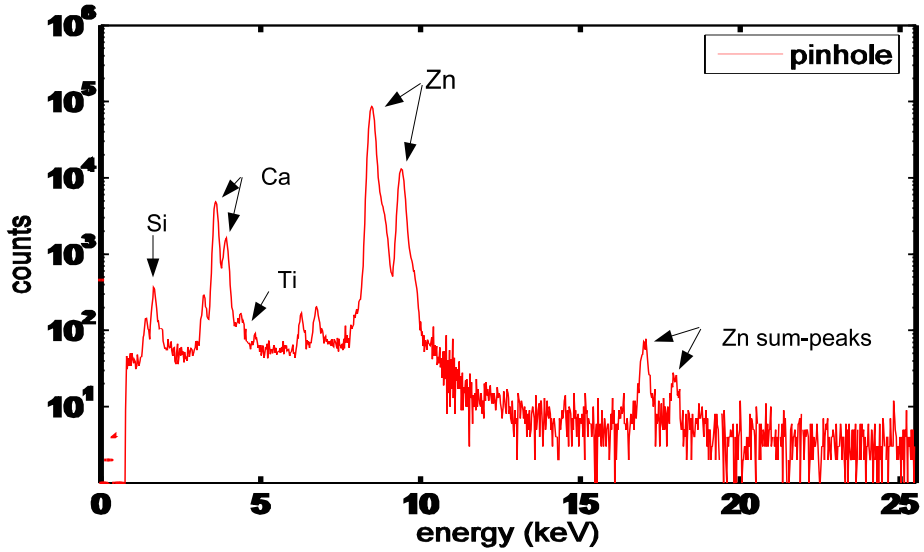

Figure 3.8 Spectrum of Zinc White showing major elements

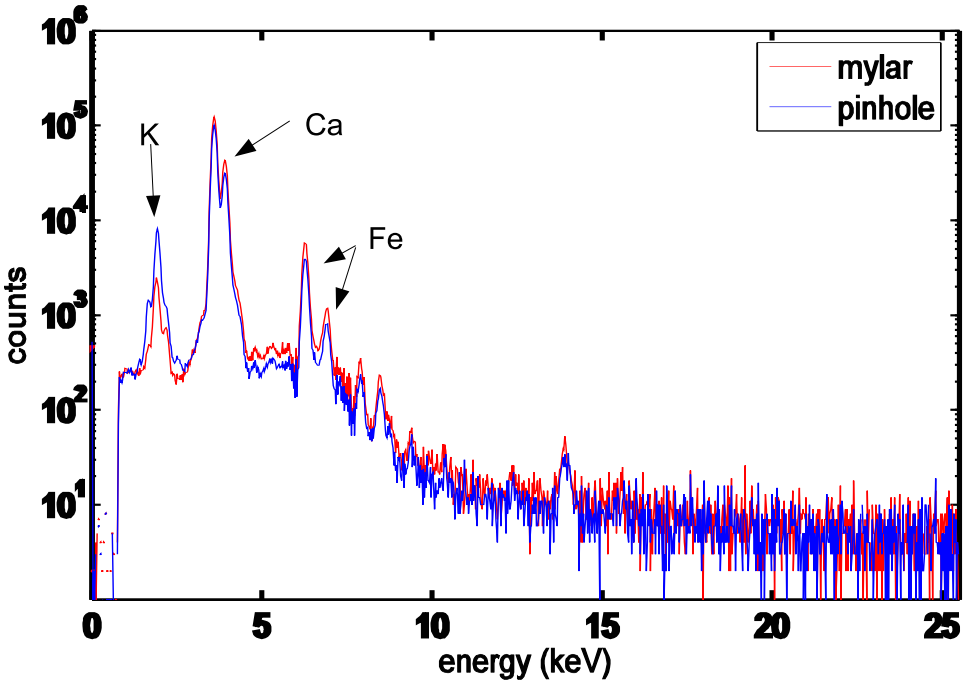

Figure 3.9 Spectrum of Ivory Black showing major elements

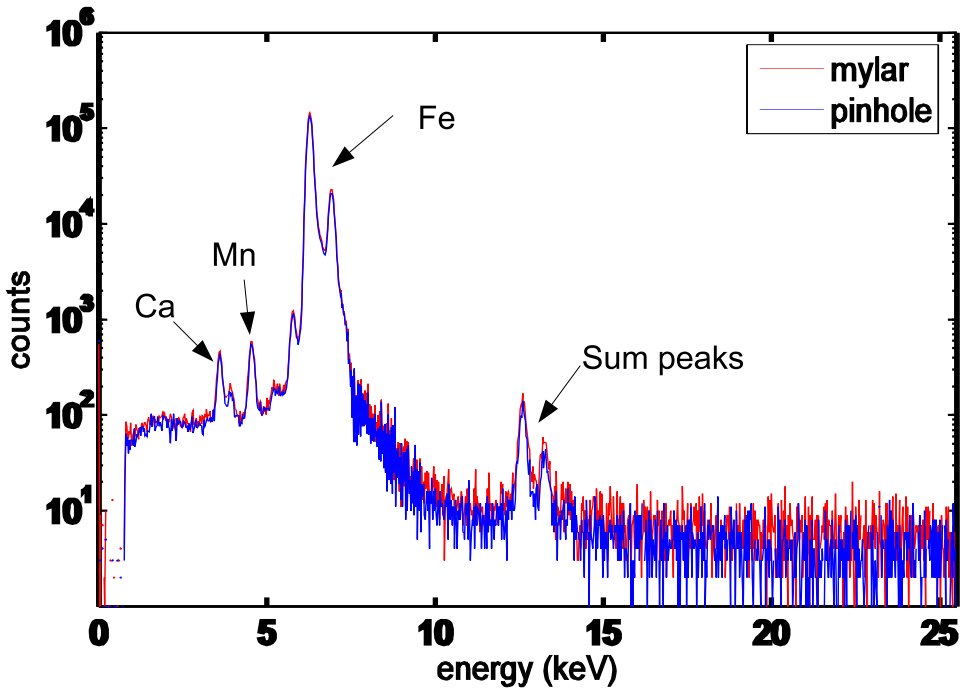

Figure 3.10 Spectrum of Mars Black showing major elements

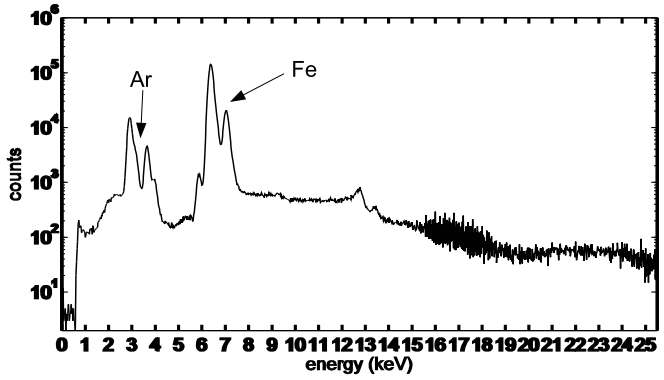

Figure 3.11 Spectrum of Mars Black run externally

3.1.6 Selected spectra of external targets

The spectra of the solid-color targets run externally match those run internally except for one peak—that of argon. The argon peak present in all the external targets but in none of the internal ones is due to the presence of small amounts of atmospheric argon in the helium-filled bag; this argon is ionized by the beam between exiting the beam line and striking the target. The other difference is the presence of a higher level of background due to laxer preparation techniques (section 2.3). Shown are the spectra for Mars Black (Fig. 3.11) and Chromium Oxide Green (Fig. 3.12). The spectrum for Mars Black shows a higher-than-normal background level due to charging (discussed in section 3.4). The mixed-color spectra require some additional explanation. In addition to sharing the argon peak with the solid-color targets, they have the expected peaks from the titanium white pigment that was mixed with the colored one to form the pastel color. For example, the spectrum for the mixture of Chromium Oxide Green and Titanium White shows substantial peaks for calcium, titanium, and zinc in addition to the atmospheric argon peak.

It is also notable that the spectra show no trace of the board used as a substrate for the paints. Even a relatively thin single layer of paint is too thick for 2 MeV

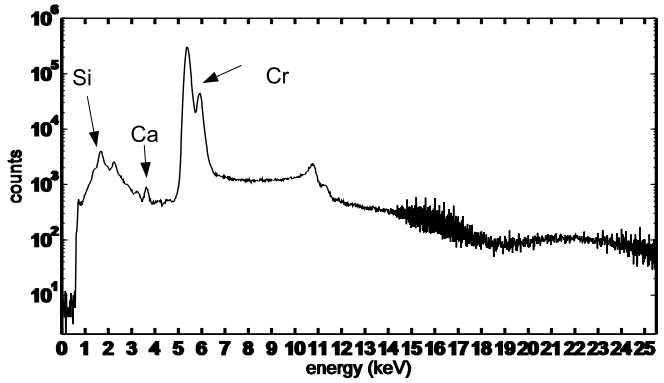

Figure 3.12 Spectrum of Chromium Oxide Green run externally

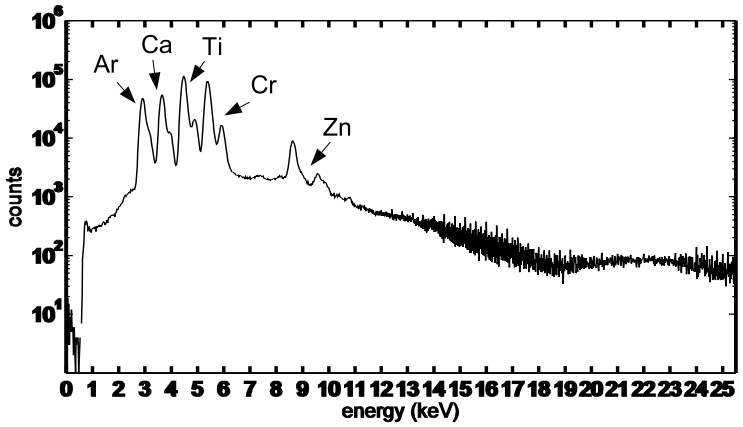

Figure 3.13 Spectrum of Chromium Oxide Green mixed with Titanium White

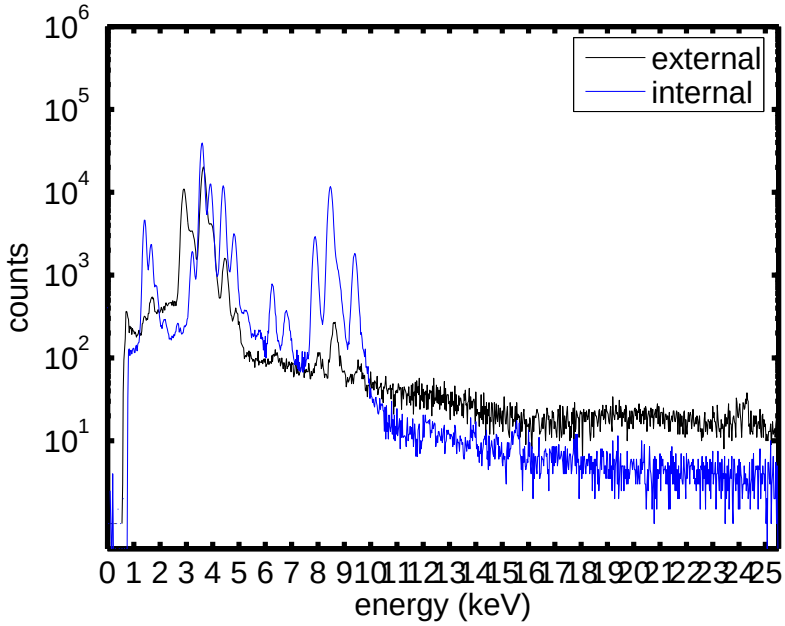

Figure 3.14 Comparison of spectra obtained internally and externally for pigment Manganese Blue; example of proper matching

protons to penetrate—thus analysis can be carried out without fear of contamination from the substrate (canvas, wood, etc.) upon which the paint is laid.

3.2 Comparisons: external and internal

The test of the baseline lies in comparisons. This is done at two levels—first by overlaying spectra in MATLAB, and second by comparing the output of GUPIX. The two methods give comparable results. Selected spectra are compared in this section; all comparison of concentrations are done in the appendix.

We give two examples of spectrum matching—one good, and one bad. First we compare the spectra of Manganese Blue obtained internally to the one obtained externally (Fig. 3.14). As is shown in the spectrum, all the peaks found internally are found externally; additionally argon is present externally with a argon-caused

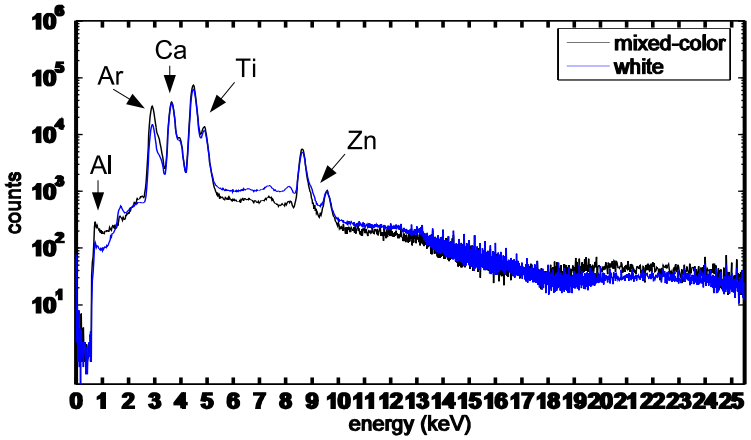

Figure 3.15 Comparison of spectra for mixed Primary Red with Titanium White showing an inability to resolve the pigments

silicon-escape peak at 0.9 keV. The relative heights of the peaks correlate—the zinc Kα peak at 8.5 keV is approximately 5 times as prominent as the copper Kα peak at 8 keV in both internally and externally-obtained spectra. All the single-color external targets match their respective internal targets with similar precision.

An example of a pigment that cannot be resolved with present methods is the mixture of Primary Red with Titanium White. As Fig. 3.15 shows, the mixed spectrum cannot be differentiated from the plain white spectrum. Both were obtained externally, so both show an argon peak and have similar background levels. The pigment Ivory Black also exhibits this problem.

3.3 Drawing conclusions

We have shown that the spectra from targets produced under strict controls (section 2.2) correlate accurately to spectra of single-color targets prepared under normal artistic conditions (section 2.3) and analyzed externally. Six of the eight mixed-color targets are resolvable into their constituent pigments (colored pigment plus Titanium

White). Only Primary Red and Ivory Black were unresolvable—their constituents are the same as the constituents of Titanium White. We were able to accurately match six of the eight mixed-color targets to their constituent parts and were also able to match all the single-color targets run externally to their internally-run counterparts.

3.4 Shortcomings of present research and suggestions for further research

We admit that there are some significant limitations involved with the present research. First, we were unable to make most of the baseline targets reliably thin enough to allow accurate counting of the charge deposited on target. This restricts the analysis to relative compositions (the abundance of one element relative to the others). This also restricts our sensitivity. There is a partial work-around for this problem—we measure the current with no target in the beam and calculate that the integrated charge is approximately the exposure time times current. This gives a better idea of the charge deposited on target and thus allows GUPIX to fit the data better. The only total solution would be to make the targets thinner by depositing less material on each target frame.

A second limitation is that our technique and accelerator are incapable of detecting layering. The exact distance any individual proton penetrates is not well defined, so inhomogeneities throughout the depth substantially affect the output. This is not a problem for the present work because all samples were homogenous. However, real paintings are commonly layered, with pigments overlayed on each other. Our equipment cannot resolve these layers. The only solution for this is to use various differential techniques—running the same target at multiple energies (thus varying the penetration depth) and building a depth profile. We refer the reader to the

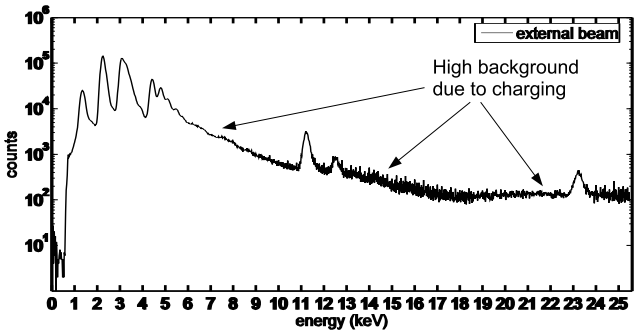

Figure 3.16 Spectrum of pigment showing high background levels at high energies

references for more detail [9–11].

A third problem, especially common in the external regime, is charging. As charge builds up in a non-conducting target, electrons jump from the environment to the target, producing Bremsstrahlung X rays that dramatically increase the background seen by the detector. Fig. 3.16 shows the characteristics of this charging background. Most solutions to this problem involve coating the surface with some conductive material such as carbon—this, however, is not feasible for paintings since it would cause damage. One feasible work-around is to run the targets for a long time under very low beam current ($<$ 2 nA).

We suggest that future work be done on actually creating a sizable database of pigments. This will be best done in conjunction with a chemist and an art historian—the chemist to formulate the pigments according to the art historian's formulas. In doing so, we propose that several questions be investigated: whether there are pigments characteristic of painting epoch, and what elements correspond to these pigments.

We have thus shown that it is possible to predict the composition of paint with a baseline database analyzed under the internal-beam regime. Much work remains before a comprehensive such database can be constructed and used, but we are con-

fident that future researchers will find our methodology and results useful in creating databases and analyzing paintings using external and internal-beam particle-induced x-ray emission spectroscopy.

Appendix A

Appendix

A.1 H-value corrections

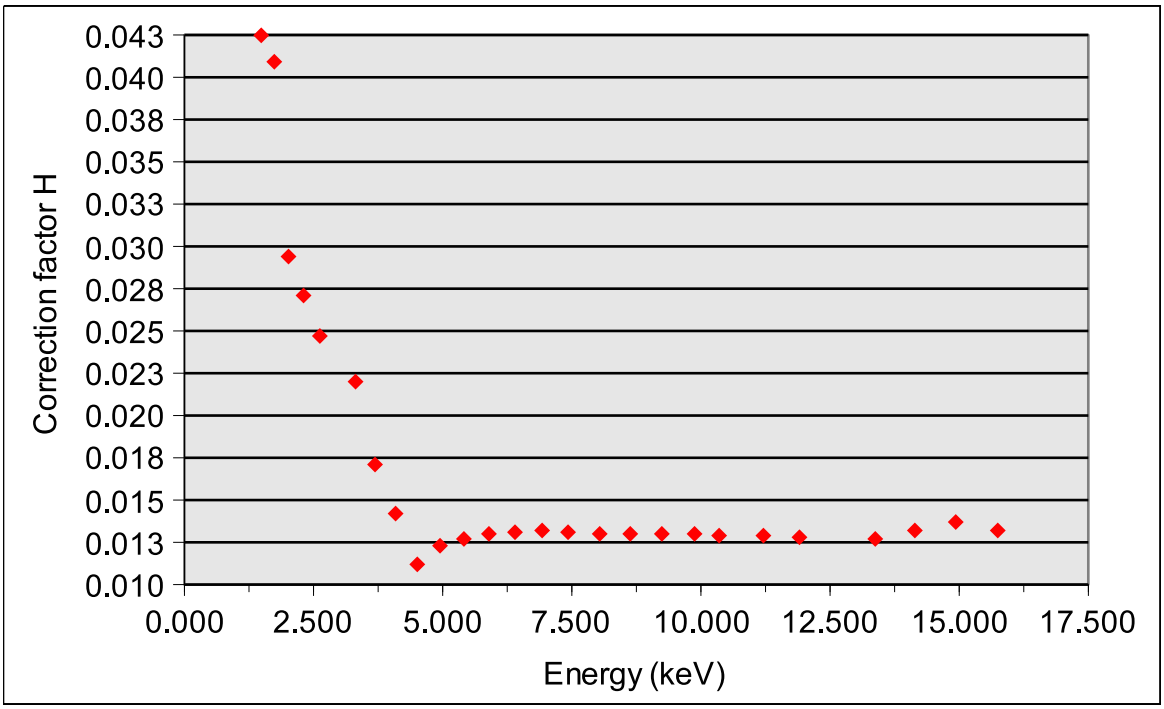

Figure A.1 H-value correction chart for pinhole filter

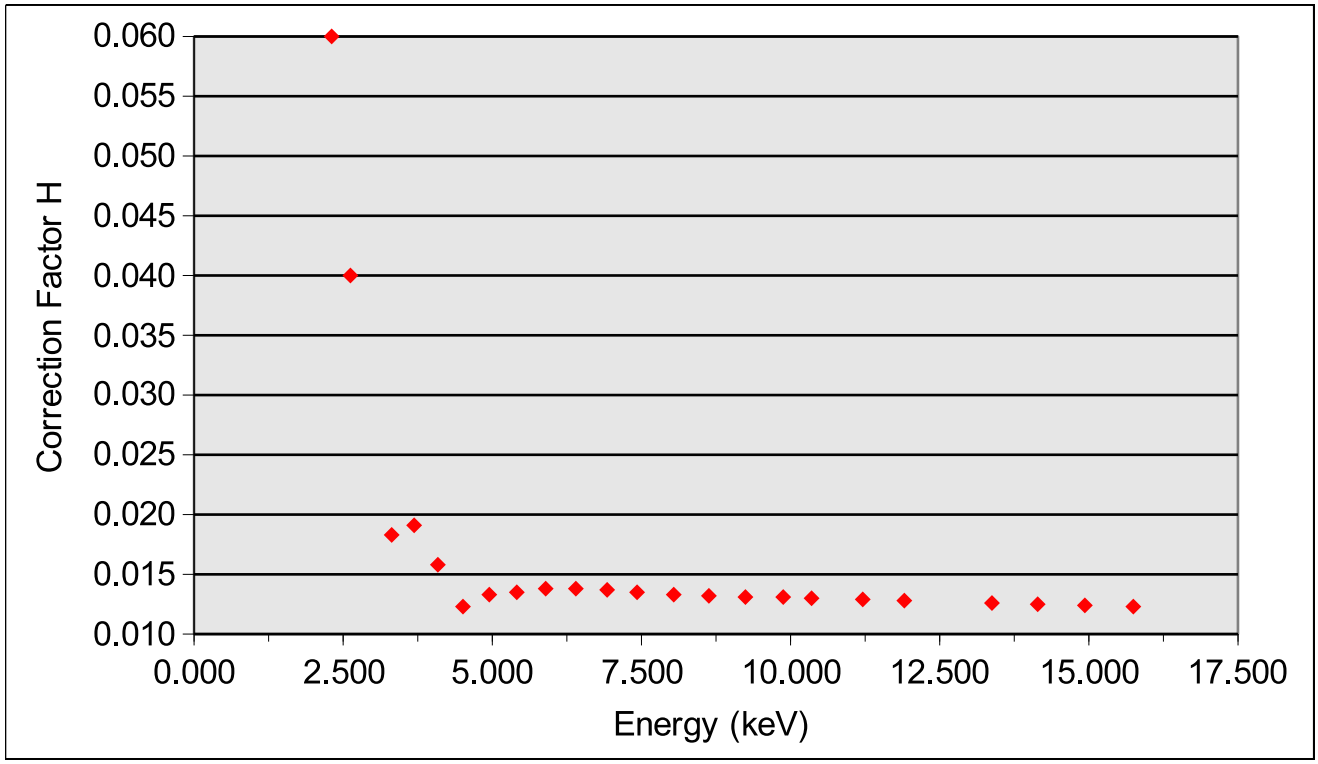

Figure A.2 H-value correction chart for mylar filter

A.2 Elemental composition tables

In this appendix section are presented tables of the elemental concentrations reported by GUPIX and corrected for nonuniform sensitivity as reported in section 2.5.

Element	**concentration (ppm)**	% **error**
Potassium	366.7	2.34
Calcium	352.0	0.78
Titanium	4.9	3.48
Manganese	0.1	35.7
Iron	1.78	1.80
Cobalt	0.3	7.38
Zinc	0.6	3.62

Table A.1 Elemental composition of Primary Red as reported by GUPIX

Element	**concentration (ppm)**	% **error**
Sulfur	368e7	2.14
Potassium	250.1	5.25
Calcium	7.6	12.5
Titanium	52.4	0.59
Zinc	0.5	1.87
Selenium	40.2	0.25
Krypton	1.3	11.6
Zirconium	0.3	11.5
Cadmium	147.4	0.77
Cesium	81.1	3.12

Table A.2 Elemental composition of Cadmium Red as reported by GUPIX

Element	**concentration** (ppm)	% **error**
Aluminum	841.4	0.58
Silicon	141.6	1.11
Potassium	48.7	1.23
Calcium	766.9	0.16
Titanium	149.4	0.29
Chromium	1.0	8.04
Iron	6.2	1.48
Cobalt	2.6	3.66
Copper	49.2	0.54
Zinc	246.7	0.27

Table A.3 Elemental composition of Manganese Blue as reported by GUPIX

Element	**concentration (ppm)**	% **error**
Aluminum	51.8	6.02
Sulfur	3.5	19.4
Chlorine	3.4	20.4
Calcium	0.8	35.0
Titanium	1.4	22.3
Manganese	2.2	11.4
Iron	2557.6	0.09
Nickel	8.1	7.24
Copper	3.7	7.15

Table A.4 Elemental composition of Prussian Blue as reported by GUPIX

Element	**concentration (ppm)**	% **error**
Potassium	1022.3	15.51
Titanium	5.1	53.1
Chromium	11058.4	0.10
Iron	14.6	8.23
Cobalt	3.17	13.7

Table A.5 Elemental composition of Chromium Oxide Green as reported by GUPIX

Element	**concentration (ppm)**	% **error**
Calcium	17.6	5.68
Titanium	1.1	29.0
Chromium	2248.8	0.130
Iron	18.7	2.91
Zinc	2.0	11.8

Table A.6 Elemental composition of Viridian as reported by GUPIX

Element	**concentration (ppm)**	% **error**
Aluminum	54.8	9.39
Silicon	37.6	5.5
Chlorine	5.6	30.4
Potassium	14.0	7.38
Calcium	523.7	0.40
Titanium	2320.0	0.14
Iron	2.4	7.59
Zinc	1632	0.58

Table A.7 Elemental composition of Titanium White as reported by GUPIX

Element	**concentration (ppm)**	% **error**
Aluminum	527.3	8.86
Silicon	662.7	3.36
Potassium	193.4	4.76
Calcium	3016.3	0.64
Titanium	32.4	10.3
Iron	30.2	6.78
Zinc	57917.0	0.14

Table A.8 Elemental composition of Zinc White as reported by GUPIX

Element	**concentration (ppm)**	% **error**
Silicon	101.6	4.54
Phosphorus	584.7	0.75
Sulfur	18.7	11.8
Chlorine	11.1	10.4
Potassium	9.0	16.6
Calcium	3294.6	0.13
Titanium	2.0	25.3
Iron	61.8	0.68
Cobalt	1.7	21.9
Nickel	1.1	19.2
Copper	4.9	4.36
Zinc	4.5	5.02

Table A.9 Elemental composition of Ivory Black as reported by GUPIX

Element	**concentration (ppm)**	% **error**
Phosphorus	4.29	28.8
Calcium	28.2	3.50
Titanium	2.8	29.9
Manganese	34.9	2.31
Iron	5647.0	0.39
Nickel	11.4	13.1
Copper	4.2	14.7

Table A.10 Elemental composition of Mars Black as reported by GUPIX

Bibliography

[1] T. Rousseau, "The Stylistic Detection of Forgeries," The Metropolitan Museum of Art Bulletin: Art Forgery **26,** 247–252 (1968).

[2] R. Sablatnig, P. Kammerer, and E. Zolda, "Structural analysis of paintings based on brush strokes," In *Proc. SPIE Scientific Detection of Fakery in Art, Walter McCrone; Duane R. Chartier; Richard J. Weiss; Eds.*, **3315,** 87–98 (1998).

[3] *Pigment handbook v. 3 Characterization and physical relationships*, T. C. Patton, ed., (John Wiley and Sons, New York, NY, 1973).

[4] N. Eastaugh, V. Walsh, T. Chaplin, and R. Siddall, *Pigment Composition: Optical Microscopy of Historical Pigments* (Elsiver, Oxford, England, 2004).

[5] O. Enguita, T. Calderon, M. T. Fernandez-Jimenez, P. Beneitez, A. Millan, and G. Garcia, "Damage induced by proton irradiation in carbonate based natural painting pigments," Nuclear Instruments section B **219-20,** 53–56 (2004).

[6] P. M. Mando, "Advantages and limitations of external beams in applications to arts and archaeology, geology and environmental-problems," Nuclear Instruments section B **85,** 815–823 (1994).

[7] N. Grassi, in *Composition and stratigraphy of the paint layers: investigation on the Madonna dei Fusi by ion beam analysis techniques*, R. Salimbeni and L. Pezzati, eds., (SPIE, 2005), No. 1, p. 58570P.

[8] M. Sanchez del Ryoa *et al.*, "Microanalysis study of archaeological mural samples containing Maya blue pigment," Spectrochimica Acta Part B **59,** 1619 1625 (2004).

[9] A. Denker, W. Bohne, J. L. Campbell, P. Heide, T. Hopman, J. A. Maxwell, J. Optiz-Coutureau, J. Raushenberg, J. Rohrich, and E. Strub, "High-energy PIXE using very energetic protons: quantitative analysis and cross-sections," X-ray Spectrometry **34,** 376–380 (2005).

[10] G. Grime, F. Watt, A. Dubal, and M. Menu, "Nuclear microscopy of inhomogenious thick samples," Nuclear Instruments section B **54,** 353–362 (1991).

[11] C. Neelmeijer and M. Mader, "The merits of particle induced X-ray emission in revealing painting techniques," Nuclear Instruments section B **189,** 293–302 (2002).